Synchrotron-based X-ray fluorescence, imaging and elemental mapping from biological samples

D V RAO[1,*], M SWAPNA[2], R CESAREO[3], A BRUNETTI[3], T AKATSUKA[4], T YUASA[4], T TAKEDA[5] and G E GIGANTE[6]

[1]Department of Physics, Sir C R Reddy Autonomous College, Eluru 534 007, India
[2]Department of Physics, Sri Durga Malleswari Siddhartha Mahila Kalasala, Bunder Road, Vijayawada 520 010, India
[3]Istituto di Matematica e Fisica, Università degli Studi di Sassari, Via Vienna 2, 07100 Sassari, Italy
[4]Department of Bio-System Engineering, Faculty of Engineering, Yamagata University, Yonezawa, Japan
[5]Institute of Clinical Medicine, University of Tsukuba, Tsukuba, Japan
[6]Dipartimento di Fisica, Universita di Roma, "La Sapienza" 00185, Roma, Italy
*Corresponding author. E-mail: donepudi_venkateswararao@rediffmail.com

Abstract. The present study utilized the new hard X-ray microspectroscopy beamline facility, X27A, available at NSLS, BNL, USA, for elemental mapping. This facility provided the primary beam in a small spot of the order of ∼10 μm, for focussing. With this spatial resolution and high flux throughput, the synchrotron-based X-ray fluorescent intensities for Mn, Fe, Zn, Cr, Ti and Cu were measured using a liquid-nitrogen-cooled 13-element energy-dispersive high-purity germanium detector. The sample is scanned in a 'step-and-repeat' mode for fast elemental mapping measurements and generated elemental maps at 8, 10 and 12 keV, from a small animal shell (snail). The accumulated trace elements, from these biological samples, in small areas have been identified. Analysis of the small areas will be better suited to establish the physiology of metals in specific structures like small animal shell and the distribution of other elements.

Keywords. X-ray fluorescence; synchrotron-based excitation; imaging; elemental mapping; biological samples.

**PACS Nos** 78.70.En; 29.20.dk; 87.59.-e; 82.80.Ej

1. Introduction

The brightness and intensity of synchrotron X-rays are many orders of magnitude more than X-rays produced in conventional X-ray tubes. This source of radiation is characterized by high collimation (small angular divergence of the beam), low emittance (the product of the source cross-section and solid angle of emission is small), widely tunable in energy/wavelength by monochromatization (sub eV up to the MeV range), high level

of polarization (linear or ellipitical) and pulsed light emission (pulse durations at or below 1 ns or a billionth of a second). It has become an indispensable tool in a wide range of research fields. The combination of high flux and low divergence provided by synchrotron source has proved to be crucial for the enormous success of experiments in the field of synchrotron-based X-ray fluorescence. We utilized the synchrotron-based X-ray microprobe system for elemental mapping [1].

Majority of studies have been carried out on plant materials, and comparatively little on invertebrates, amphibians, fish, and other affected wildlife [2]. It is interesting to choose the invertebrates, because among living organisms, for example, snails represent most of the biomass in the world due to their small size for easy dispersal by land and water with their metabolic versatility and flexibility and their ability to tolerate even unfavourable conditions. External and internal structures of invertebrates, such as small animal shell (snail), is important for our understanding of this diverse shelled animal group, which carry a strong biological signal and incorporate a broader range of calcium carbonate into their biological structure. These are aquatic, with a majority living in shallow marine waters and feed mainly on algae and decaying matter. The tissue layer of a snail which overlies the body and secretes the shell is known as mantle. The microorganisms from these serve as excellent models for understanding all living systems. Trace elements from these samples are fundamental intrinsic components of the biological systems. Paleobiological studies are necessary to know more about the developmental and evolutionary changes occur over millions of years, such as, living organisms of invertebrates [3–10].

2. Experimental method

A top-view schematic of the X27A experimental end-station lay-out is shown in figure 1 (information describing the facility can be found at http://www.nsls.bnl.gov). The X27A microprobe end-station is located approximately 10.8 m from the dipole bending-magnet port (6-mrad opening angle) on the NSLS 2.8 GeV X-ray storage. The X-rays were achromatically microfocussed onto the sample using dynamically bent rhodium-coated Kirkpatrick–Baez (KB) mirrors. The microfocussing mirrors consisted of 20 cm long (17.2 cm usable mirror length) trapezoidal-shaped single crystal silicon substrates polished to a roughness better than 1 Å rms (root-mean-square). The energy range from ~4 to 32 keV could be accessed through a combination of silicon (111) and (311) channel-cut monochromators. The sample under investigation was mounted on motorized (sub-micron resolution) translation and rotation stages and raster-scanned through the microfocussed X-ray beam. The X-rays were focussed at a distance of 9 cm from the end of the mirror enclosure, to a FWHM spot size of ~6 μm (vertical) × 17 μm (horizontal). Another 1 cm long ionization chamber was used to monitor the X-ray intensity just before the sample, for normalization purposes. Depending upon the X-ray energy range in use, sufficient signal was obtained from these small-length ionization chambers by flowing appropriate gases through them. Measurements of the X-ray flux at the sample position were continuously recorded during the experiment using the ionization chambers and/or silicon photodiode, and were found to be around 20% lower than the calculated values.
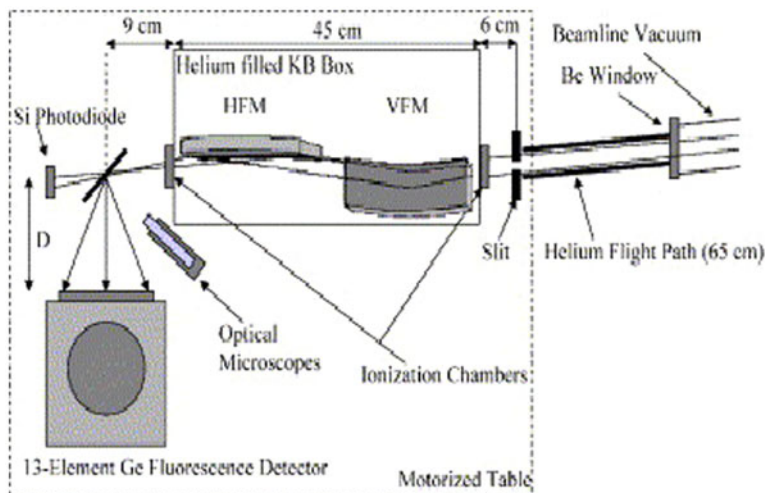
Figure 1. Top-view schematic of the X27A microprobe end-station. VFM and HFM are the vertical and horizontal focussing KB mirrors, respectively. The sample is viewed using optical microscopes and the transmitted X-rays are detected using a silicon photodiode. Fluorescence X-rays are collected with the 13-element liquid nitrogen-cooled germanium detector. The distance from the sample to this detector, D, is varied using a motorized linear slide. There is a total experimental air path (between beryllium window and sample location) of 15 cm.

The sample was typically oriented in normal direction to the direction of X-ray propagation and at 45° horizontal incidence angle. Fluorescence radiation was measured using a liquid-nitrogen cooled 13-element germanium detector, located in the horizontal plane of the synchrotron ring and at 90° to the X-ray beam direction, thus reducing the scattered radiation from entering the detector. Each detector element was circular with a diameter of 1 cm. The detector was mounted on a motorized linear slide so that the detector–sample distance could be adjusted. The detector system employed digital processing electronics, and a FWHM energy resolution at 5.895 keV of ∼180 eV was measured for a shaping time of 6 μs (averaged over the whole detector array). With a sampling time of 1 μs, the detector could easily run at input count rates exceeding 5×10^4 cps per detector element, with a corresponding FWHM resolution at 5.895 keV of ∼260 eV. The end-station, on vibrational damping air pads, was housed upon a motorized 6-axis experimental honeycomb table, thus allowing the whole assembly to be positioned vertically, to optimize for a particular energy range of interest, or translated laterally to intercept silicon (111) or (311) monochromatic radiation. Experimental table was raised or lowered to match the focussed beam position on the sample for each excitation energy and the subsequent scan section was performed. In this way, the experimental table was not continuously scanned but adjusted only when beam motion became significant (e.g. 50% of the vertical focussed beam size). With these improvements, the microprobe sensitivity and the detector count rate capability have improved the limits of detection
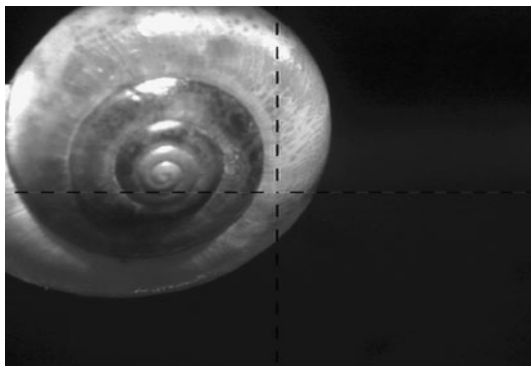
Figure 2. The physical dimension of the sample used and the scanning area for 8, 10 and 12 keV.

for the synchrotron-based X-ray fluorescence [11]. Figure 2 shows the physical dimension of the sample and the scanning area used for point scan imaging. Fresh samples of invertebrates (snails) of various sizes, which contain considerable biological soft tissue, were collected in winter before spawning occurred to avoid the associated loss of biomass. These samples were packed in teflon containers and stored. The samples were checked for any leakage of the soft tissue from the boundaries of the shell before mapping at different energies. The scanning area was considered, nearer to the origin of the apex, where most of the soft-tissue was occupied, covering 80% of the relevant area of the sample.

3. Results

Elemental mapping is a straightforward approach. It records full synchrotron-based X-ray fluorescence spectrum at each scan point, integrate over spectral ROIs corresponding to specific elemental X-ray fluorescence lines. Only a small animal shell sample is needed for the measurement and no special sample preparation is necessary. The sample was mounted on a computer-controlled sample stage and could be rotated or moved relative to the X-ray beam in x-, y- and z-directions with increments of 1 μm. Correlated stage movement and spectrum acquisition allow the collection of $n(x) \times n(y)$ individual X-ray fluorescence spectra. $n(x)$ and $n(y)$ are the number of pixels in horizontal and vertical directions of the image, respectively which during or after the acquisition can be processed to yield net elemental maps and line profiles. The X-ray beam hit the specimen at 45°. An energy-dispersive detector was placed at 90° towards the incoming beam. This angle provides the best peak-to-background ratio. The elemental mapping was performed by exciting pixel by pixel in the sample. The two-dimensional selected area for scanning (figure 3) was a representative part of the sample and covered approximately three-fourth of the sample.

A motorized stage which moved the sample through the X-ray beam and fluorescence data were collected with a step of 1 μs in horizontal and vertical directions with 1 s integration time. The X-ray fluorescent intensities for Mn, Fe, Zn, Cr, Ti and Cu were
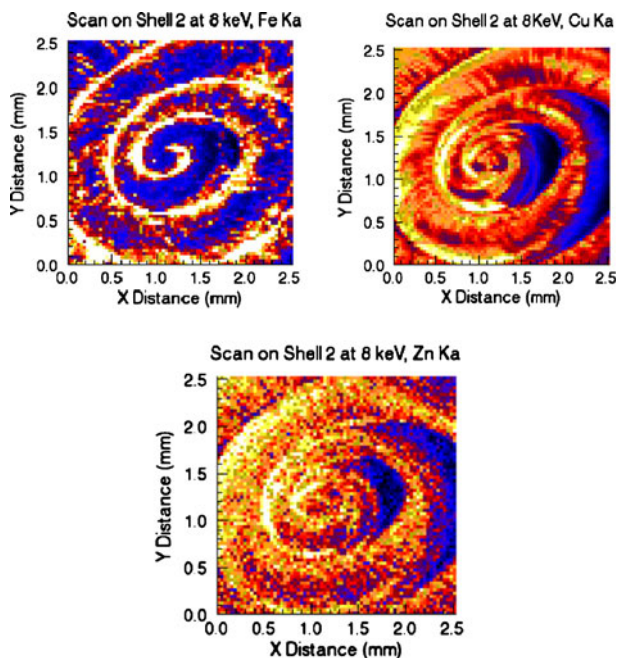
Figure 3. X-ray fluorescent elemental maps for Fe, Cu and Zn with 8 keV synchrotron X-rays.

measured using a liquid-nitrogen-cooled 13-element energy-dispersive high-purity germanium detector, and the sample was scanned in a 'step-and-repeat' mode. With 1 μs integration time per point, larger areas of the sample could be scanned without loss of spatial resolution. This is important, as physiologically relevant areas (soft-tissue distribution within the shell), are non-uniformly distributed to few millimetres. This resulted in many thousands of points in a step-and-repeat mode, and the total time required for each elemental map at fixed excitation energy was varied from 8 to 12 h. An optical microscopic photograph of the sample with soft-tissue is shown in figure 4. Histomorphological observations showed that a large part of the tissues had turned black. It was thought that change of colours resulted from the living tissue due to the presence of other materials. The data analysis was performed using the IDLVirtual Mechine 6.3 programmes. The programme utilizes the signals needed for normalization, e.g. ionization chamber signals, detector dead time and the ring current [12].

The experimental results of elemental maps are shown in figures 2–5. In these figures, the elemental distributions were graded using a continuous colour bar. Arbitrary colour bars were assigned to each elemental level, red being the highest, yellow moderate and blue the lowest to moderately large at higher energies. Figures 2–5 show the counts of the X-ray intensity. This way, the inner chambers of the sample were highlighted in elemental maps, suggesting that the experimental procedure as well as data analysis were successful in a purely justification manner with IDL programmes. The K_α X-ray intensities of
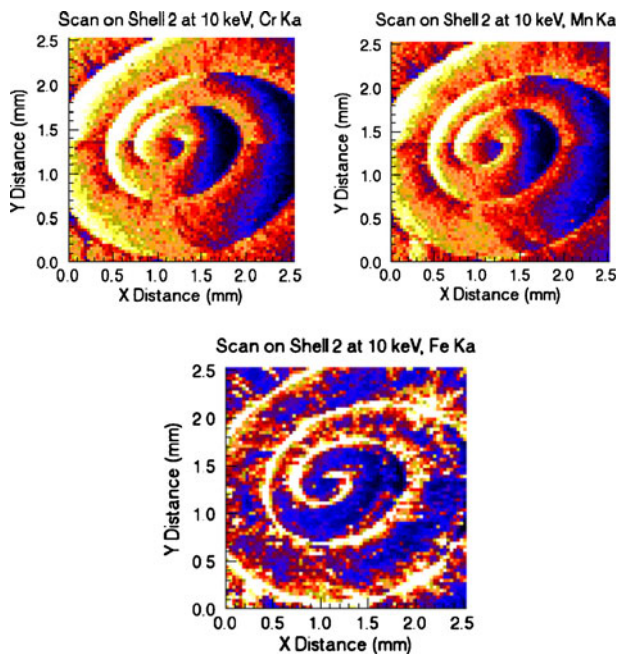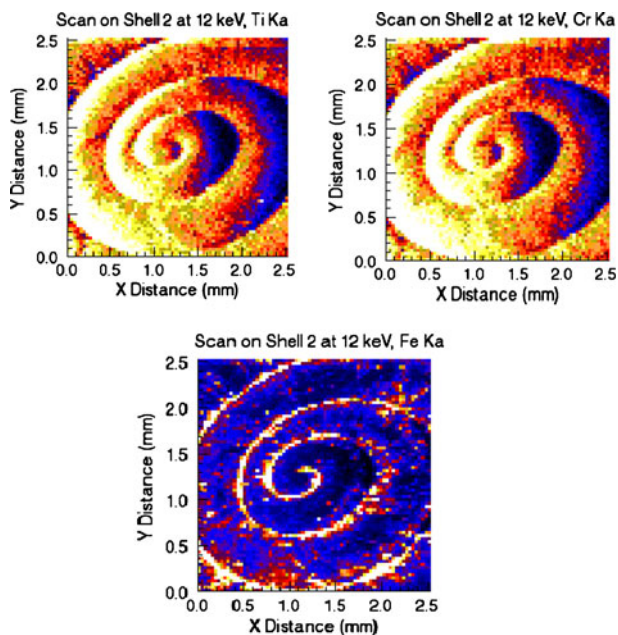
Figure 4. X-ray fluorescent elemental maps for Cr, Mn and Fe with 10 keV synchrotron X-rays.

Mn, Fe, Zn, Cr, Ti and Cu were processed. From this, two-dimensional distributions of fluorescent intensities were mapped. They were normalized with respect to the intensity of the incident X-rays. According to the results shown in figures 3–5, the distributions of Ca, at 8, 10 and 12 keV, is same, and the distribution of Ti, Cr and Mn are in similar composition, and for Fe, Cu and Zn, the distribution changes considerably. These are inconsistent with the distribution of the soft tissue within the shell and the external structure. These images were obtained in the same dark area, with maximum distribution of the soft tissue. Figure 6 shows the isosurface of the sample at 8 keV. Figure 7 shows the correlation plots at 8 keV for a few elements. The X-ray fluorescence spectra of the measured points are shown in figure 8 without any absorption corrections at 10 keV. This way, for example, the contribution of Ca lines is assessed over the scattered radiation. The process is continued for other elements in the region of interest from pixel to pixel on the sample.

The distribution ratio of the peak areas of Mn, Fe, Zn, Cr, Ti and Cu, which were calculated from the spectra, revealed that there were significant differences in the distribution ratios of the dark and bright areas of the sample. All images were of 10 μm resolution and the measurement time was 1 s per point. The ratio from the fluorescent X-ray intensities of Mn, Fe, Zn, Cr, Ti and Cu measured in the bright area was comparatively higher than that in the dark area. The chemical states of these in the dark and bright areas will be analysed in the near future using XANES. The distribution of elements is clearly seen on

Figure 5. X-ray fluorescent elemental maps for Ti, Cr and Fe with 12 keV synchrotron X-rays.

all the samples. Note that the levels of Ca were the highest among the elements shown and the result was consistent at 8, 10 and 12 keV excitation energies. However, the darker areas were dominated by the soft tissues surrounded by the external shell and overlapped with other elemental map distributions.

The distributions of the X-ray fluorescence intensities were obtained from Ca at 8, 10 and 12 keV. No effort was made to quantify the results in terms of element concentrations. Ca bound maps helped to show that the sample's external structure had the highest distribution of Ca. The Mn distribution closely matched that of Ca. This suggests that Mn
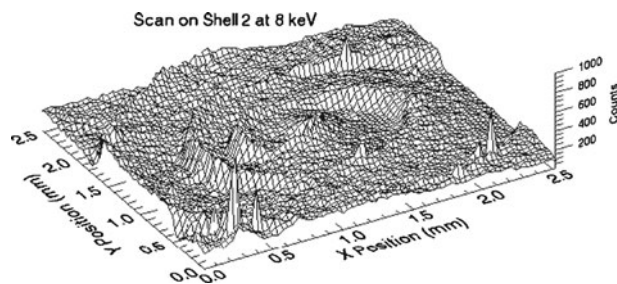
Figure 6. Isosurface at 8 keV (Fe K_α, Mn K_α and Zn K_α) in the *x*-direction and *y*-direction, and the number of counts on the *z*-direction.
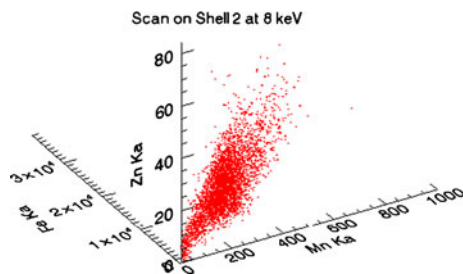
Figure 7. Correlation plot for Fe K$_\alpha$, Mn K$_\alpha$ and Zn K$_\alpha$ at 8 keV.

serves the same structural function as Ca. Ca and Mn, although not displaying a completely uniform distribution, were the most evenly distributed metals examined in the study. Analysis of the small areas will be better suited to establish the physiology of metals in specific structures like small animal shell. The predominant element of interest for this study is calcium; however, the maps for other elements are presented to demonstrate the capabilities of the technique. It can be appreciated that the maps obtained for calcium are much clear. This is due to the weak attenuation of the X-rays through the embedded soft tissue.

4. Conclusions

Elemental maps were generated from the small animal shell (snail), using 8, 10 and 12 keV synchrotron X-rays, and the distribution of Ca map demonstrated the anatomical
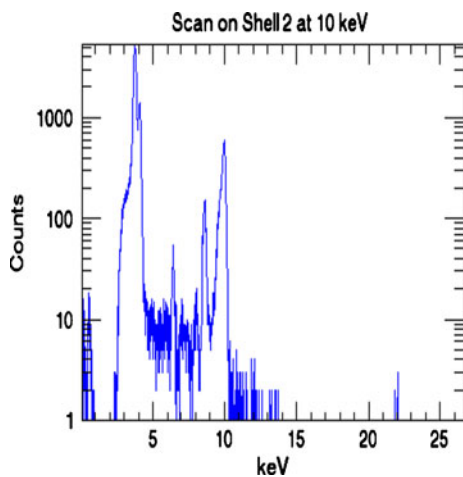
Figure 8. The excited fluorescence spectrum at 10 keV, from one of the ROIs at a pixel in the map. This way Ca K$_\alpha$ and K$_\beta$ lines are identified, lying over the scattered radiation.

structure. Thus, application of synchrotron-based X-ray fluorescence to biological tissue provided robust qualitative data about the behaviour and effect of metals and metalloids. The mapping capability essentially provided a picture of the elemental distribution within the material, which very easily provided a tremendous amount of information. In biological applications the maps may give a direct and clear observation of element occurrences in different regions of the sample. Elemental maps depicting the local concentration of a certain element have great potential in biomedical research, because of its low detection limit and its high spatial resolution. The spatial distribution of trace elements in tissues is involved in many biological functions of living organisms. In general, biological samples are low atomic number (Z) matrices, which have less backscattering and lower spectral baselines, higher sensitivity, and significantly less self-absorption of X-rays by the sample. As a result, synchrotron-based X-ray fluorescence is rapidly becoming a powerful research tool in biogeochemical research.

Acknowledgements

References

[1] R Van Grieken and A A Markowikz, *Handbook of X-ray spectrometry* (Marcel Dekker, New York, 1993)
[2] T Punshon, B P Jackson, A Lanzirotti, W A Hopkins, P M Bertsch and J Burger, *Spec. Lett.* **38**, 343 (2005)
[3] K P Koutzenogii, T I Savchenko, O V Chankina, A G Kovalskaya, L P Osipova and A V Bgatov, *J. Trace. Microprobe. Tech.* **21(2)**, 311 (2003)
[4] J D'Amore *et al*, *J. Environ. Qual.* **34**, 1707 (2005)
[5] K G Scheckel *et al*, *Environ. Sci. Technol.* **38**, 2792 (2004)
[6] D G Schulze *et al*, *Phytopathology* **85**, 990 (1995)
[7] P M Bertsch and D B Hunter, *Chem. Rev.* **101**, 1809 (2001)
[8] A Manceau, M A Marcus and N Tamura, *Rev. Mineral. Geochem.* **49**, 431 (2002)
[9] S R Sutton *et al*, *Rev. Sci. Mineral. Geochem.* **49**, 429 (2002)
[10] D B Hunter, P M Bertsch, K M Kemmer and S B Clark, *J. De Phys. IV.* **7(C2)**, 767 (1997)
[11] http://www.nsls.bnl.gov/X27A
[12] J M Ablett, C C Kao, R J Reeder, Y Tang and A Lanzirotti, *Nucl. Instrum. Methods.* **A562**, 487 (2006)